JOURNAL OF GEOPHYSICAL RESEARCH, VOL. 102, NO. D24, PAGES 29,555–29,566, DECEMBER 26, 1997

Transmission of solar radiation in boreal conifer forests: Measurements and models

Wenge Ni, Xiaowen Li, and Curtis E. Woodcock
Department of Geography and Center for Remote Sensing, Boston University, Boston, Massachusetts

Jean-Louis Roujean
GAME/CNRM (Meteo France, CNRS), Toulouse, France

Robert E. Davis
Cold Regions Research Engineering Laboratory, U.S. Army Corps of Engineers, Hanover, New Hampshire

Abstract. A combined geometric-optical and radiative transfer (GORT) model allows incorporation of multiple scales of clustering in conifer canopies on the estimation of radiation transmission. Consideration of clustering of branches into whorls is the latest addition to this model. Modification of the GORT model to include whorl orientation improves the ability to model the observed patterns of solar radiation transmission as a function of solar zenith angle and height in the canopy. Whorl orientation distributions are derived from multidirectional measurements using a geometric optical mutual shadowing model. For BOREAS test stands, model estimates and vertical measurements of photosynthetically active radiation transmittance within the canopy show (1) general decreases in transmission as solar zenith angles increase in the range of solar zenith angles dominated by beam irradiance, (2) increases in PAR transmission at very high solar zenith angles where diffuse skylight is dominant, (3) maximum scattering and absorption occur in the middle of the canopy. Model estimates match measurements from the forest floor, indicating the value of the model for providing radiation inputs to snowmelt models in forested landscapes.

1. Introduction

The Boreal Ecosystem-Atmosphere Study (BOREAS) has been undertaken to improve our understanding of the interactions between the boreal forest biome and the atmosphere and to clarify their role in global climate change [*Sellers et al.*, 1995]. These interactions include the exchanges of mass, energy, and momentum between the boreal forest and the lower atmosphere. The radiation regime above, within, and below the boreal forest canopy plays a crucial role in many dimensions of atmosphere-vegetation interactions. First, light interception and absorption are closely related to photosynthesis [*Sellers*, 1985, 1987], which directly influences the exchange of carbon between the forest canopy and the atmosphere. Second, absorption of solar radiation by leaves and the ground surface in turn heats the surrounding air, which when combined with the roughness of the vegetated surface results in the turbulence that transports mass and energy between the biosphere and the atmosphere. Studies of the effect of the forest canopy on turbulent transport have shown that the vertical distribution of solar radiation absorption by canopy elements is essential for predicting the momentum, heat, and energy transfer patterns within and just above plant canopies [*Ni*, 1997]. Third, radiation transmitted to the forest floor provides energy for snowmelt, which in turn provides moisture for soils and plants. All these indicate that a clear understanding of the radiation regime in conifer stands contributes directly to the objectives of BOREAS.

The complex architecture of conifer forests results in strong landscape heterogeneity with respect to radiation at many spatial scales since a light ray may be trapped in or transferred through any element of the canopy. Currently, a limited understanding of the radiation environment within snow-covered boreal landscapes leads to large uncertainties in the surface radiation inputs used in climate, hydrology, and vegetation interaction studies [*Bonan et al.*, 1995].

The purpose of this paper is to pursue an improved understanding of the effects of conifer canopy structure on the radiation regime within and below boreal conifer forests, with the primary motivation being to provide inputs to snowmelt models (see *Hardy et al.* [this issue]). This study involves both theoretical models and field measurements of the radiation transmission in BOREAS test sites. While this paper focuses on results in specific stands, our long-term research develops models useful to spatially distributed models of snow processes over time periods of seasons [*Davis et al.*, this issue].

2. Background

Radiation transmission in a plant canopy is affected by many factors, including the source distribution (proportions of incident beam irradiance and diffuse skylight and its spectral properties), the canopy structure, as well as the spectral properties of the canopy elements and the canopy background. The proportions of beam irradiance and diffuse skylight and its spectral properties depend on atmospheric conditions. Radiation

Paper number 97JD00198.
0148-0227/97/97JD-00198$09.00

transmission differs for irradiance at different solar zenith angles and also for diffuse skylight. Because of high absorption by plants in the visible wavelengths (0.4–0.7 μm), radiation interception approaches the absorption, and multiple scattering can be ignored [*Roujean*, 1996]. Because of the high leaf albedo in the near infrared, especially combined with the high surface albedo in the snow-covered BOREAS sites during the winter, multiple scattering in the canopy layer and the multiple bouncing between the canopy layer and the ground surface have to be taken into account.

A complete description of a canopy requires the specification of the position, size, and orientation of each element in the canopy, which has proven to be complicated and impractical. Usually statistical parameters of canopy structure, such as the leaf area index (LAI), leaf angle distribution (LAD), and the spatial arrangement of canopy foliage, branches, and stems are used in mathematical models to describe light penetration through a forest canopy [*Campbell and Norman*, 1989].

The effect of LAI and LAD on the radiation regime for horizontally homogeneous plant canopies is well developed (see the review by *Ross* [1981]). The canopy gap probability (or Beer's law) was first used by *Monsi and Saeki* [1953] to describe the beam penetration. The gap probability was defined as the probability that a beam misses a set of randomly located leaves. Meanwhile the effect of the spatial arrangement of canopy elements (called dispersion structure) was also modeled by a radiative transfer (RT) approach. Usually random and clumped patterns were used to describe the dispersion structure of plants. As suggested by *Ross* [1981], for random dispersion structure, there is an equal probability of finding a plant at any location, and for clumped dispersion structure, the probability of finding a plant at a given location is related to the presence or absence of plants in the surrounding area. For the random dispersion model, the only inputs are LAI and LAD, as used in the RT approach. For canopies with clumped leaves, a negative binomial model was used to describe the beam penetration [*Nilson*, 1971].

Conifer canopies exhibit hierarchical clumping structure, including the clumping of needles into shoots, shoots into branches, branches into whorls, whorls into crowns, with crowns comprising the canopy. One higher level of clumping is the grouping of individual crowns into patches (or stands), which then comprise the landscape [*Urban et al.*, 1987]. All these levels of clumping contribute to heterogeneity in the radiation environment in conifer forest. This conceptual model for a forested landscape is central to our efforts to distribute physical models at the scale of stands across landscapes.

Various levels of the clumping that occurs in conifer forests have been incorporated into the RT approach for modeling the effects of conifer structure on the radiation regime [*Norman and Jarvis*, 1974, 1975; *Nilson*, 1971; *Oker-Blom et al.*, 1983, 1991]. A two-level clumping model was developed by *Norman and Jarvis* [1974, 1975], which includes the clumping of needles into shoots and shoots into whorls in a Sitka spruce forest. This model not only considered the effect of the clumping on the directly transmitted radiation but also the scattered transmittance at any spectral range and any solar zenith angle. Their study concluded that the highly clumped structure tends to allow more direct beam radiation to pass through the canopy unintercepted. At the same time clumping of the needles into shoots made the shoot foliage elements appear less translucent. Their model was complicated, requiring detailed canopy structure measurements such as the location and number of whorls, the orientation and length of shoots.

Studies by *Oker-Blom et al.* [1983, 1991] showed that the effects of foliage clumping into crowns and crowns into a canopy allow more light to pass through to the lower part of the canopy. The light condition was to a high degree determined by tree structure. This effect seems especially true for sparse canopies. Similar results were obtained through an empirical approach by *Sampson and Smith* [1993], in which the canopy gaps were measured by a spherical densiometer. They found a reasonably good loglinear fit for the between-crown gap probability as a function of the stem count density and average basal area of live crown.

A three-dimensional radiative transfer model [*Kimes et al.*, 1985] was also applied to a pine forest canopy to account for the unique radiative transfers that take place in forests due to the effects of clumps of tree crowns [*Kimes et al.*, 1986]. They found that this clumping structure has two effects on the radiative transfer within the canopy: one is the increase of the gap probability to the understory and/or soil layer that increases the influence of the scattering properties of these lower layers, and the other is the increase of the number of low transmitting clumps of vegetation within the scene causing increased backscatter and decreased forward scatter relative to the homogeneous case.

While much has been learned about the radiation environment in plant canopies using radiative transfer approaches, the basic assumption of a horizontal homogeneous layer is limiting for canopies that exhibit a high degree of clumping [*Oker-Blom et al.*, 1991]. An alternative approach that has proven useful for discontinuous canopies uses geometric optics. The geometric-optical (GO) approach has been developed primarily for modeling canopy reflectance in discontinuous vegetation canopies [*Li and Strahler*, 1985, 1992; *Strahler and Jupp*, 1990]. A forest canopy is treated as an assemblage of three-dimensional tree crowns of specified shape and size, and the directional reflectance over the canopy is the linear combination of the product of the areal proportions and the spectral signatures for four scene components: sunlit crown surface, sunlit ground surface, shaded crown surface, and shaded ground surface. The areal proportion of each component is a function of the crown shape, crown size and count density, as well as illumination and viewing angles. Hence the GO approach captures the basic features of discontinuous canopies, for example, the clumping of foliage into crowns which cast shadows.

In this study, a new model [*Li et al.*, 1995] that combines the geometric-optical and radiative-transfer (GORT) approaches is used to model the effect of conifer canopy structure on solar radiation transmission in BOREAS test sites. This approach has the advantage of the strengths of both the RT and the GO approaches. All theoretical models are abstracts of reality and as such require basic assumptions about reality. The assumptions underlying this study are as follows:

1. Shoots are considered as the basic canopy elements, based on previous studies that have shown shoots to be the basic scattering and photosynthetic elements in conifer forests [*Oker-Blom et al.*, 1991; *Chen*, 1996]. Shoots are assumed randomly distributed within the confines of a whorl [*Norman and Jarvis*, 1975]. The foliage-area-volume-density parameter used in this study includes the effect of the shoots, stems, branches, and trunks [*Chen*, 1996].

2. An earlier study by *Norman and Jarvis* [1975], field measurements [*Chen*, 1996], and the results of tree parameter

retrieval [*Li and Strahler*, 1996] in BOREAS test sites all indicate that the horizontal whorls within a single crown act somewhat like a pile of horizontally oriented disks [*Ross and Marshak*, 1991] within an ellipsoid envelope. In this study, a horizontal whorl structure is assumed for conifer trees, and the effects of the horizontal whorl structure on the radiation regime is considered.

3. The focus is on the effects of the canopy structure on the radiation regime at the scale of forest stands. Within stands, trees are assumed randomly distributed [*Oker-Blom et al.*, 1991]. The radiation regime is characterized by the mean stem count density, mean size of tree crowns with a specified ellipsoid shape, and with specified foliage spectral properties.

3. Modeling Transmission of Solar Radiation

Contributions to the distribution of total radiation within the forest canopy come from three sources: (1) beam irradiance through gaps, (2) diffuse skylight through gaps, and (3) solar radiation scattered by the canopy elements and understory background. The basic approach used is to estimate the first two components by gap probabilities between canopy elements based on geometric optics, while the third component is estimated using a radiative transfer approach. The effect of the clumping of foliage elements into crowns is incorporated into the RT approach through leakage factors.

3.1. Gap Probabilities

The gap probability for a canopy is defined as the probability of a photon reaching a given point located at a certain height in the canopy without being scattered. As described earlier, for a horizontally homogeneous canopy layer, the gap probability is described by Beer's law. For sparse canopies the clumping of leaves into crowns yields a nonuniform distribution of gaps. In fact, some proportion of light will pass through the canopy without passing through tree crowns (referred to as between-crown gaps), while another proportion may pass through crowns without being scattered (within-crown gaps). Beer's law fails to describe these in discontinuous canopies.

In the GORT model, the discontinuous canopy layer is modeled as an assemblage of randomly distributed tree crowns of ellipsoidal shape, having horizontal crown radius R and vertical crown radius b and centered between heights h_1 and h_2, where h_1 and h_2 are the lower and upper bounds of crown center height. The crown count volume density λ_v is equal to $(\lambda/h_2 - h_1$, where λ is the stem count density in square meters. Within each single crown, the foliage and branches are assumed to be uniformly distributed. The penetration of the incoming direct and diffuse irradiance is described by the summation of two types of gap probabilities: the between-crown gap probability and the within-crown gap probability (see Figure 1). The between-crown gap probability $P(n = 0|h, \theta_i)$ for direct beam radiation describes the proportion of the direct solar beam at solar zenith angle θ_i that reaches a point located at height h without passing through any crowns (i.e., $n = 0$). This is the probability that there are no crown centers within the beam projected cylinder volume V_Γ with a radius R starting from the top of the canopy layer to level h, otherwise the beam will pass through crowns. On the basis of Boolean theory the between-crown gap probability can be expressed as an exponential function of crown number within the volume V_Γ, that is,

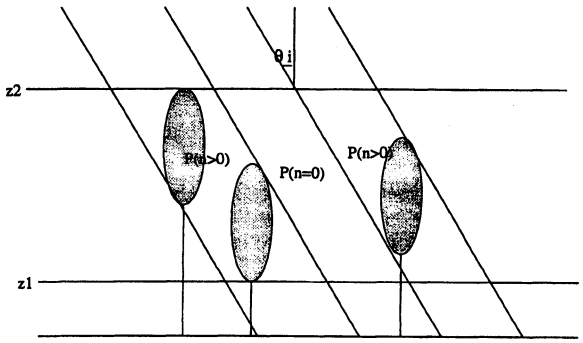

Figure 1. Vertical cross section of a canopy showing the distribution of tree crown heights, as modeled in geometrical-optical and radiative transfer (GORT). Between-crown gap probability at height h is related to the volume V_Γ, and within-crown gap probability at height h is related to the location (point I at height z) where a beam enters a crown and volume V_β, and h_1 and h_2 are the lower and upper bounds of crown center height.

$$P(n = 0|h, \theta_i) = e^{-\lambda_v V_\Gamma} \tag{1}$$

The within-crown gap probability $P(n > 0|h, \theta_i)$ is defined as the proportion of direct beam radiation passing through at least one crown without being scattered. The gap probability for diffuse skylight, or the "openness factor," is the integral of the gap probability for the direct beam over the hemisphere. The calculation of the within-crown gap probability is rather complicated. With the assumption of randomly distributed foliage within a single crown, the within-crown gap probability $P(n > 0|h, \theta_i)$ can be described by Beer's law, but the within-crown pathlength s is a random variable, since the location where a beam enters a crown, the number of crowns through which it passes, and the pathlength through an individual crown are random. The within-crown gap probability is

$$P(n > 0|h, \theta_i) = \int_0^\infty P(s|h, \theta_i) e^{-\tau(\theta_i)s}\, ds \tag{2}$$

where $\tau(\theta_i) = k(\theta_i)F_a$, where $k(\theta_i)$ is the leaf area projection factor at angle θ_i, and F_a is the foliage area volume density within a single crown, where shoots, stems, branches, and trunks are all included. We have $F_a = L_a/\lambda V_{\text{crown}}$, where L_a is the effective leaf area index, i.e., after considering the clumping effect of needle into shoots [*Chen et al.*, 1991], and V_{crown} is the volume of a single crown; s is the within-crown pathlength, and $P(s|h, \theta_i)$ is the within-crown pathlength distribution, which depends on the location where a beam enters the canopy crowns, the number of crowns through which it passes, and the mean pathlength within a single crown,

$$P(s|h, \theta_i) = \int_h^{h_2} \sum_{n=1}^{n=\infty} (P(s|n, z, h, \theta_i) P(n|z, h, \theta_i))\, dz \tag{3}$$

where $P(s|n, z, h, \theta_i)$ is the within-crown pathlength distribution for solar rays entering crowns at height z at angle θ_i, then passing through n crowns to height h. It can be obtained with the basis of the between-crown gap probability. The probability, $P(n|z, h, \theta_i)$, is the distribution of numbers of crowns intercepted by a beam incident at θ_i and entering crowns at height z, then traveling to height h. We can also easily get the

formula with the assumption of a Poisson distribution of the number of crowns centered in volume V_β; here V_β is the beam projected cylinder volume with radius R starting from the entering point at level z to the level h. The details for the calculation of the between-crown and within-crown gap probabilities can be found in the work of *Li et al.* [1995].

As discussed, it can be seen that with the GO approach, the between-crown gap probability is characterized by the size, shape, and density of crowns. Through combination of the GO and RT approaches, the within-crown gap probability is therefore not only described by the L_e but also by the size, shape, and density of crowns.

3.2. Effect of Horizontal Whorl Structure

For conifer forests the clumping of shoots into horizontal whorls of branches results in a nonrandom distribution of canopy elements within crowns. The existence of a horizontal whorl structure allows more light to pass through the canopy without being scattered, particularly at larger solar zenith angles. To model the effect of the horizontal whorl structure, the calculation of the gap probabilities as described above has to be modified. For randomly distributed foliage within crowns with the assumption of "solid" crowns, the between-crown gap probability was calculated on the basis of the probability that there are no crowns centered within the beam projected cylinder volume V_Γ; that is, the probability that the point M at height h will not be shadowed in the horizontal plane at h. However, given the horizontal whorls distribution of within crowns, there is less chance that the point M will be shadowed. The between-crown gap probability has to be modified in order to include the horizontal whorl effect. A correcting factor $G_b(\theta_i)$, describing the distribution of the whorl orientation structure, is introduced here. It is defined as the proportion of shadowing area of the nonsolid crown (with horizontal whorl branch structure) over the projected area of the "solid" crown at solar zenith angle θ at a plane. The modified formula for calculating the between-crown gap probability is

$$P(n = 0|h, \theta_i) = e^{-G_b(\theta_i)\lambda_v V_\Gamma} \quad (4)$$

3.3. Properties of Predicted Gap Probabilities

Figure 2 shows the modeled between-crown and within-crown gap probabilities from the original GORT model, using tree geometry parameters and foliage area volume density in the old jack pine stand in the southern study area (SOJP) of BOREAS as inputs. It shows that (1) the between-crown gap probability decreases with distance from the top of the canopy and at a faster rate at larger solar zenith angles, which means that more light will be intercepted at the upper part of the canopy at larger solar zenith angles; (2) the within-crown gap probability has a maximum value in the middle of the canopy layer, with larger values at larger solar zenith angles; (3) the total gap probability at the top of the canopy layer for beam radiation at any solar zenith angle is primarily due to the between-crown gap probability, whereas the radiation reaching the lower part of the canopy layer at smaller solar zenith angles is the result of significant contributions by both the between-crown and the within-crown gap probabilities. Only for the bottom of the canopy at large solar zenith angles is the within-crown gap probability dominant.

Several differences between the total gap probability predicted by GORT and Beer's law are apparent in Figure 3. First, the vertical distribution from GORT resembles a logistic curve

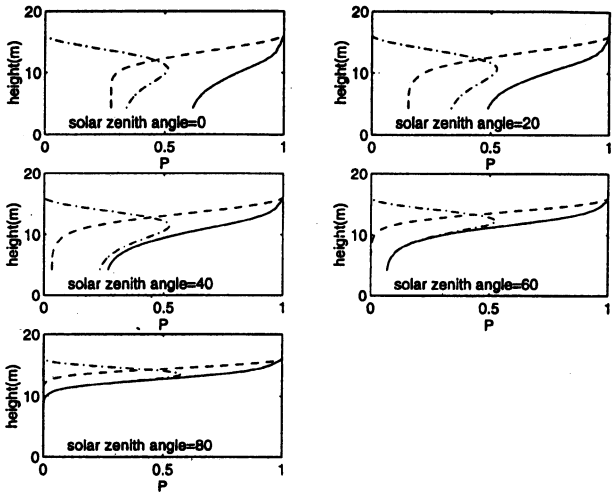

Figure 2. Gap probabilities for the SOJP site as estimated by the GORT model. Solid lines are for total gap probabilities, dashed lines are for the between-crown gap probabilities, the alternating dashed and dotted lines are for the within-crown gap probabilities.

of sigmoidal shape as a function of height, with most of the radiation intercepted between h_1 and h_2 (7.7 m and 12.7 m in this case), whereas the predictions from Beer's law are simply exponential functions. The cause of the deviation from an exponential function like Beer's law is the between-crown gap probability. Second, larger gap probabilities are predicted by GORT compared to Beer's law for beam irradiance at smaller solar zenith angles. Third, GORT and Beer's law become similar at very large solar zenith angles. The patterns of the gap probability for diffuse skylight, which are the integrated gap probabilities over the hemisphere, are shown in Figure 4. Comparison of the estimates of light interception by GORT and Beer's law (Figure 5) shows that the maximum light interception predicted by Beer's law occurs in the top of the canopy, as opposed to the middle as predicted by GORT.

Solar radiation through gaps can be modeled as the summa-

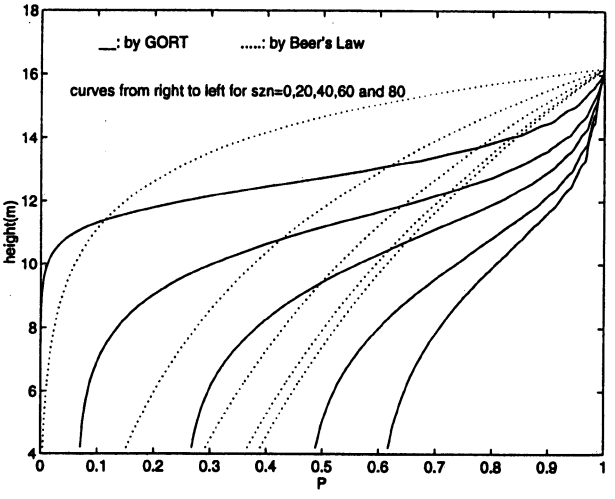

Figure 3. Comparison of gap probabilities in the SOJP stand as predicted by the GORT model and Beer's law for a variety of solar zenith angles.

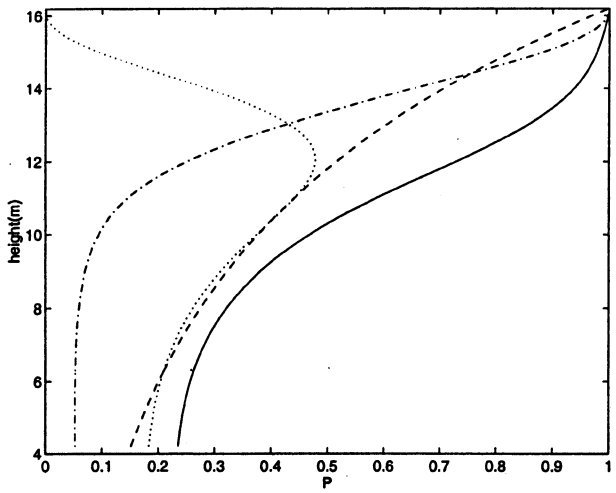

Figure 4. Gap probabilities for diffuse skylight in the SOJP stand as predicted by the GORT model and Beer's law. The dashed line is for Beer's law. The solid line is the total gap probability, the dotted line is for the within-crown gap probability, and the alternating dashed and dotted line is the between-crown gap probability.

tion of the weighted gap probabilities for direct beam and diffuse skylight. On the basis of measurements of direct beam and diffuse skylight proportion on clear days at the SOJP site, an empirical formula for calculating the proportion of the direct beam on clear days in BOREAS test sites is proposed,

$$\rho_I(\mu_i) = \frac{\mu_i}{\mu_i + 0.09} \tag{5}$$

where $\mu_i = \cos \theta_i$. Figure 6 shows the comparison between the field measurements and the curve calculated from equation (5). The curve matches reasonably well with the field measurements except for slight underestimation.

On the basis of equation (5), Figure 7 shows the first two components of solar radiation transmittance on clear days as a function of solar zenith angle by the original and modified GORT. Notice that for the modified form of GORT for

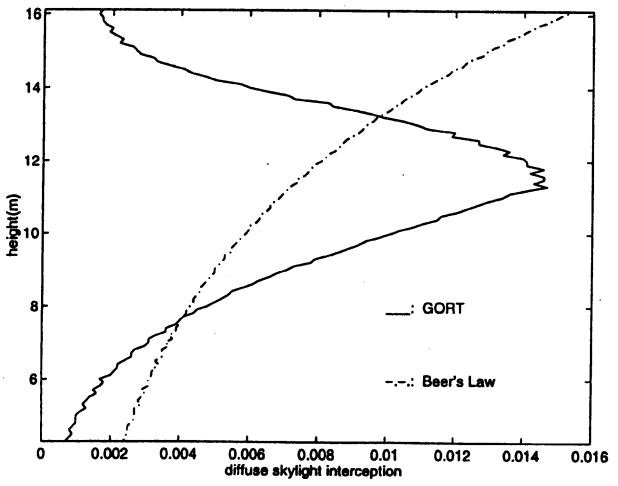

Figure 5. Diffuse skylight interception in the SOJP stand, as estimated by Beer's law and the GORT model.

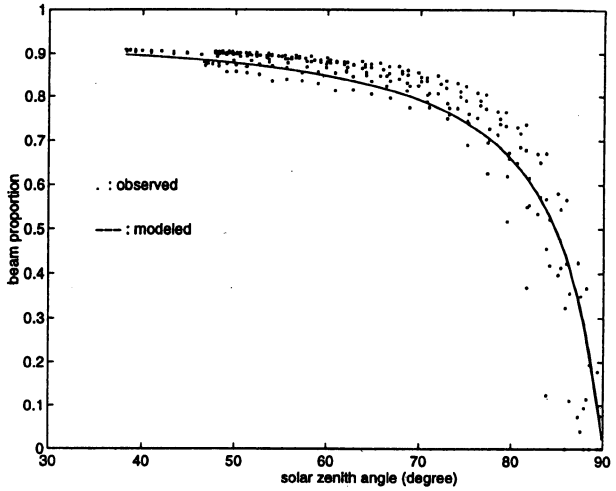

Figure 6. Proportion of total irradiance arriving at the top of the canopy uncollided (or beam irradiance) in BOREAS test sites on clear days in early April 1994.

incorporating the effect of whorls, the formula $G_b(\theta_i) = 0.7 \cos^2(\theta_i) + 0.3$ was obtained by inverting the geometric-optical mutual shadowing bidirectional canopy reflectance model [*Li and Strahler*, 1992] using PARABOLA data [*Deering*, 1995] collected over BOREAS forest sites (see a detailed description in the Appendix). Figure 7 shows (1) the beam and diffuse skylight through gaps decreases first with the increase of solar zenith angles (which is due to the increase in pathlength for beam irradiance) and then increases at very larger solar zenith angles, which is due to the increasing proportion of incident diffuse skylight at very larger solar zenith angles; (2) the modified GORT model for whorls predicts larger gap probabilities than the original, especially at larger solar zenith angles.

3.4. Multiple Scattering

The calculation of multiple scattering within the canopy and the multiple bouncing between the canopy and the background

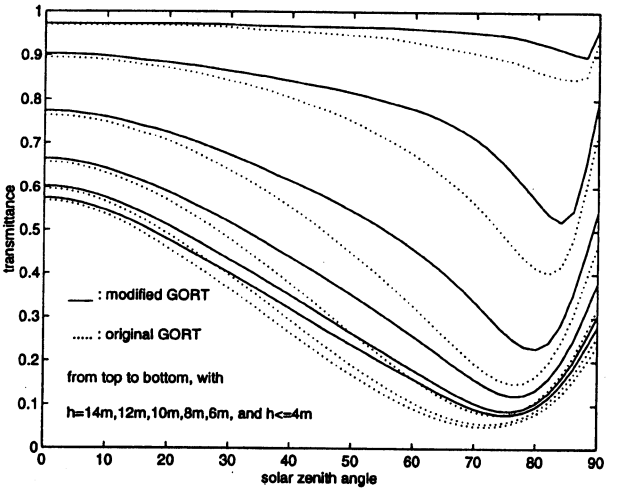

Figure 7. Gap probability as a function of solar zenith angle in the SOJP stand, as estimated by the original and modified GORT models.

Table 1. Spectral Properties of Leaf and Snow in Snow-Covered SOJP

μm	0.3–0.7	0.7–1.35	1.35–2.3	Reference
Prop1[a]	0.46	0.37	0.17	*Iqbal* [1983]
Prop2[b]	0.49	0.40	0.11	6S
Leaf albedo	0.15	0.80	0.45	ref*[c]
Snow albedo	0.95	0.50	0.00	*Dozier* [1989]

[a]Prop1, proportion of extraterrestrial solar spectral irradiance.
[b]Prop2, proportion of solar spectral irradiance at the Earth surface.
[c]ref*, *Middleton and Walter-Shea* [1995].

were modeled using a RT approach. That is, the canopy is divided into several thin layers. With the vertical distribution of gap probability calculated above, the vertical distribution of the intercepted irradiance within each thin layer can be easily obtained by the differential of the gap probability. Thus the product of the intercepted irradiance and the leaf albedo will be the single scattering sources within each thin layer. By introducing a leakage factor, the amount of single scattering leaking out through the between-crown gaps and the magnitude of scattering sources for higher orders of multiple scattering can be obtained. Then by following the RT approach, from the amount of single scattering in one certain layer to reach another layer, the second-order scattering sources can be obtained. Then the higher-order pairs of scattering are solved successively in a similar way. Through these steps, the total multiple-scattering (including downward and upward) components can be obtained by the summation of all orders of multiple scattering. The details of these calculations can be found in the work of *Li et al.* [1995].

Because of the different spectral properties of leaves and snow over the solar spectrum, it was divided as follows: 0.3–0.7 μm, 0.7–1.35 μm, and 1.35–2.3 μm, and the multiple scattering is calculated as the sum of the multiple scattering in each spectral range. The spectral leaf albedo (leaf reflectance plus leaf transmittance), snow albedo, and proportion of solar radiation in each spectral range are listed in Table 1. Prediction of the vertical distribution of the downward multiple scattering over the solar spectrum (Figure 8) shows the following: (1) peaks in the middle of the canopy, which is due to maximum

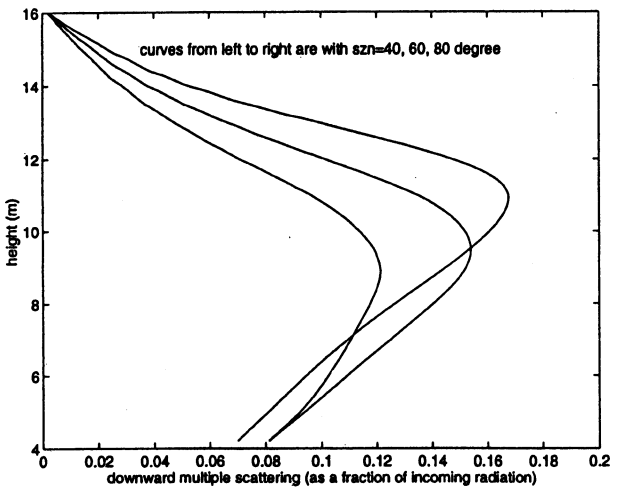

Figure 8. Predicted distribution of downward multiple scattering in the SOJP stand as estimated by the GORT model.

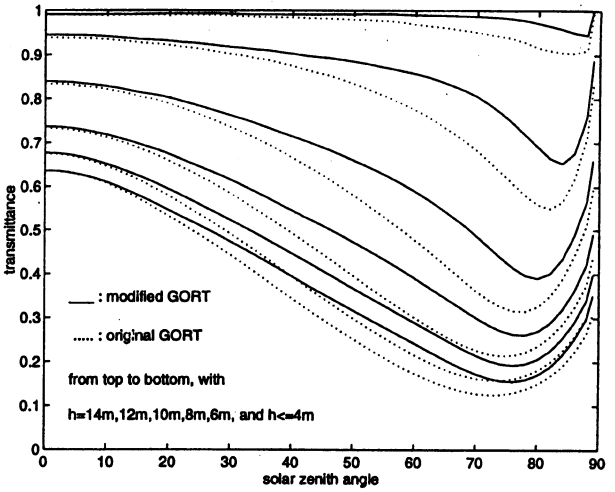

Figure 9. Predicted total solar radiation transmission in the SOJP stand as estimated by the GORT model.

radiation interception in the middle of the canopy layer; (2) as solar zenith angles increase, longer beam pathlengths lead to more light interception higher in the canopy.

Total solar radiation transmission can be modeled as the sum of the total gap probability for beam irradiance, diffuse skylight, and multiple scattering. Figure 9 shows predicted total solar radiation transmission as a function of solar zenith angle at selected heights.

4. Field Measurements

During the 1994 summer field campaign, photosynthetically active radiation (PAR) (0.4–0.7 μm) measurements were collected by setting up a 15 m mast in the old jack pine and old black spruce stands in the southern areas of BOREAS (so-called SOJP and SOBS sites). Each mast was equipped with a series of horizontal perches (or bars) at 2 m, 4 m, 6 m, 8 m, and 10 m. Each perch had six equidistant optical sensors, 0.3 m apart. The perches were oriented south, with a small angle between them to avoid mutual shadowing. The measurements were collected every 10 min from sunrise to sunset almost every day during the BOREAS summer campaign. Averaged values of the PAR measurements from the six sensors at each level were used in this study.

During the winter field campaign in 1994 in the old jack pine stand in the southern study area (SOJP site) and in 1995 in the old black spruce stand in the northern area (NOBS site), a Skye SKE 510 radiation sensor for diffuse skylight and a Fritschen Q-6 net radiometer for net radiation were mounted above the canopy to measure incoming beam and diffuse radiation. Meanwhile, 10 Eppley (PSP) pyranometers were placed randomly on the snow surface beneath the canopy within an area with a radius of 35 m for measurements of total downwelling radiation at snow surface. The random positions were determined by drawing a random number for the azimuth and distance away from the Campbell datalogger. Radiation observations were taken at 10 s intervals, averaged over a period of 10 min. Measurements were made from day 37 at 1520 to day 40 at 1630 in 1994 in SOJP and from day 81 at 1424 to day 85 at 1300 in 1995 in NOBS. Averages of the 10 pyra-

Table 2. Input Tree Parameter Values for GORT

Site	R(m)	b(m)	$\lambda\left(\frac{1}{m^2}\right)$	h_1(m)	h_2(m)	ELAI	FAVD $\frac{1}{m}$
SOJP	1.2	3.5	0.284	7.7	12.7	1.89	0.41
SOBS	0.76	2.7	0.405	3.0	8.5	2.27	0.87
NOBS	0.26	0.9	1.594	0.1	3.1	1.26	3.15

nometer measurements were used for the calculation of total solar radiation transmittance in each test site.

The tree geometry parameter values required for GORT in the three sites are shown in Table 2. For the SOJP site the trees are quite uniform in height; for example, the tree height is from 12 m to 15 m [*Chen*, 1996]. The crown shape and size (R and b) and the boundaries of crown center height (h_1 and h_2) are from *Soffer et al.* [1995]. The rest are from *Chen* [1996].

For the SOBS site the trees are not so uniform, the tree height varying between 0 and 11 m [*Chen*, 1996]. It was recorded that 60% of the trees were less than 6 m tall with a horizontal crown radius 0.7 m, 30% were between 6 m and 8 m high with a crown radius 0.8 m and 10% were between 8 m and 10.5 m high with a crown radius of 1.0 m. Because of the nonuniform distribution tree height and sizes, the input parameters h_1 and h_2 were calculated as $h_1 = \text{mean}(h_c) - \text{std}(h_c)$ and $h_2 = \text{mean}(h_c) + 3\text{std}(h_c)$, where h_c is the crown center height and mean(h_c), and std(h_c) are the mean and standard deviation of the crown center height. The stem density and ELAI data are from *Chen* [1996].

For the NOBS site an area with small trees was selected. The average tree height is around 2.15 m with a stand deviation of 1.02 m. Careful tree parameter measurements were made in this area. A 50 m × 50 m area near the pyranometers was chosen and divided into 25 (10 m × 10 m) cells. In each of five randomly selected cells, 22 trees were selected randomly, and for each of them, tree height and crown radius were measured. Additionally, counts of stems were made in each of the five cells. The results for stem count density, the horizontal and vertical crown radii, the lower and upper bounds of crown centers are given in Table 2. From the 110 sample trees the mean(h_c) = 1.61 m and std(h_c) = 0.77 m.

The foliage area volume density (FAVD) measurements were collected as follows: In each of the five randomly selected cells mentioned above, a tree was selected that was close to the average size. Five measurements (counts) of needles and twigs were made on each of the selected trees. For each measurement, a location was selected using three random numbers, which are height of sample, azimuth from tree stem, and distance from the tree stem. A 0.1 m × 0.1 m × 0.1 m hollow cube was placed at that random location on the tree. The number of the needles in the cube were counted and the dimensions of each twig within the cube were measured. From these measurements, the averaged twig area and needle area density are 0.84 (m^{-1}) and 3.72 (m^{-1}). As suggested by *Oker-Blom et al.* [1991] and *Chen* [1996], individual shoots are the basic foliage elements for conifer stands. The ratio of half the total needle area in a shoot to half the total shoot area, $\gamma_E = 1.61$ [*Chen*, 1996], was used here. The foliage area volume density (including the twigs) FAVD = $0.84 + 3.72/\gamma_E = 3.15\ m^{-1}$.

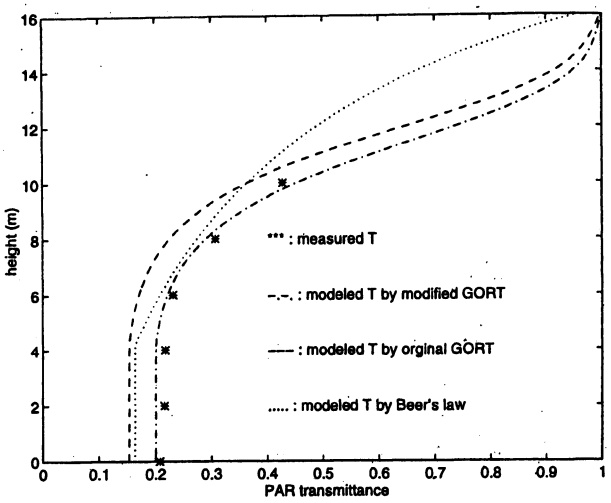

Figure 10. Comparison of modeled and measured vertical distribution of (PAR) transmission in the SOJP stand.

5. Comparison of Measurements and Model Estimates

With the tree geometry parameters described in the last section as input, GORT was run to estimate PAR and total solar radiation transmission as a function of solar zenith angle and height for comparison with the field measurements in the SOJP, SOBS, and NOBS test sites. The PAR transmission is estimated from the total gap probabilities (ignoring the multiple scattering) due to large absorption of canopy elements within the range of 0.4–0.7 μm. The total solar radiation transmission is modeled by gap probabilities and multiple scattering. As mentioned, the total solar radiation was divided into three ranges due to the different spectral properties of canopy elements and snow within each range (Table 1).

5.1. Vertical Distribution of PAR Transmission

Figures 10 and 11 show the vertical distribution of the averaged PAR transmission on clear days in the SOJP and SOBS

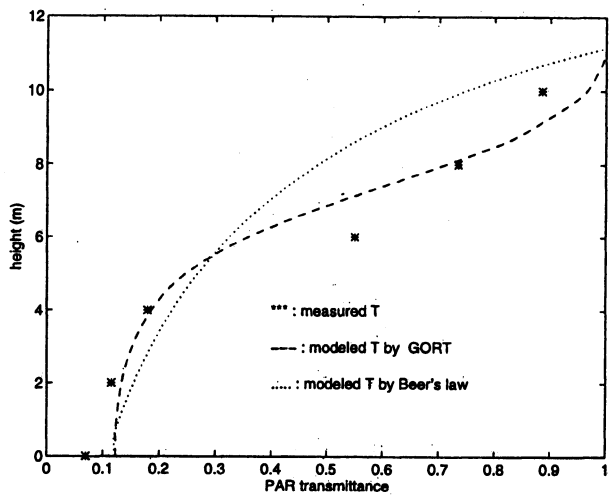

Figure 11. Comparison of modeled and measured vertical distribution of PAR transmission in the SOBS stand.

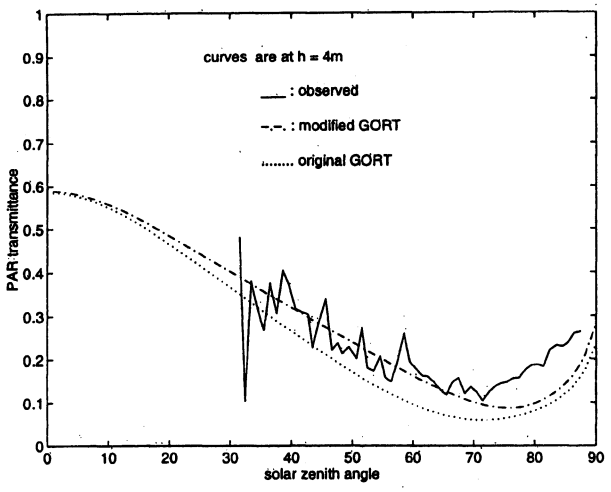

Figure 12. Comparison of modeled and measured PAR transmission as a function of solar zenith angles in the SOJP stand.

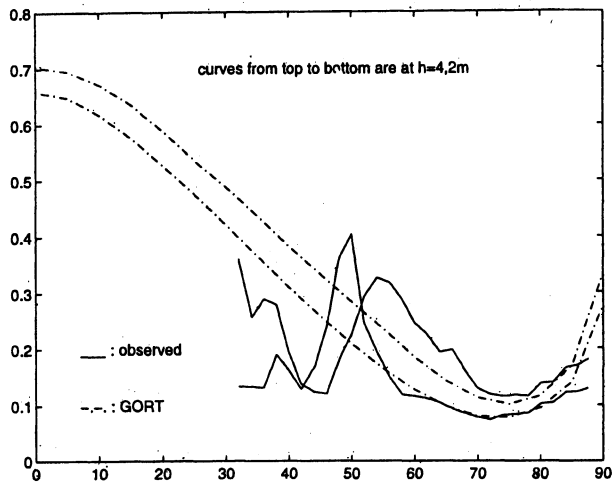

Figure 13. Comparison of modeled and measured PAR transmission as a function of solar zenith angles in the SOBS stand.

sites. Tree height is in the range of 12–15 m in the SOJP site and 0–11 m in SOBS site. The highest PAR measurements were only 10 m; this means we only had the measurements in the middle or lower part of the canopy for the SOJP site. The field measurements in the SOJP site (see Figure 10) show the lower part of the sigmoidal shape of PAR transmission and the prediction by the modified GORT matches well with the field measurements, whereas the prediction by the original GORT and Beer's law tend to underestimate the field measurements. The field measurements in the SOBS site (see Figure 11) show the whole sigmoidal shape of the vertical distribution of PAR transmittance, and the estimates from GORT match reasonably well. As expected, Beer's law fails to predict the sigmoid shape of the field measurements. Figure 11 also shows some deviation in the modeled results from GORT relative to the measurements at 6 m and 10 m. The deviation is due at least partially to the effects of crown size distributions. In the GORT model, the calculations are based on a single mean crown size, which for normally distributed or at least symmetrically distributed crown size is a reasonable approximation. For the SOBS site the crown size distribution is more lognormal, and incorporation of this effect is planned for future work and may improve the results. The deviation may also be due to the effect of improper crown shape. The cone or cone plus cylinder crown shape may be more proper for the SOBS site. Here we consider the crown as ellipsoid in the sake of simplicity, although this may yield some limitations. Given the lack of field data in the SOBS site and the noisy nature of the PAR transmission measurements collected at a single site, the effect of the horizontal whorl structure was not pursued here.

5.2. PAR Transmission As a Function of Solar Zenith Angles

Figures 12 and 13 show the PAR transmission as a function of solar zenith angle in the SOJP and SOBS sites. Because of differences in stem count density on the eastern and western sides of the mast in the SOBS site, we have only predicted PAR transmittance in the afternoon based on the stem count density on the western side of the mast. Figure 13 shows the prediction of the PAR transmission based on the stem density on the western side of the mast. The stem count density was estimated using the nearest neighbor rule [*Hammond and McCullagh*, 1974] based on an estimation of 1 m distance between trees on the western side of the mast.

The patterns in the field measurements are complex and in some ways are less than ideal for comparison as they are collected at a single site and subject to effects of individual trees rather than integrated measurements for the entire stand. For the SOJP site there are fairly dramatic changes of transmittance over small changes of solar zenith angles, which makes the data appear noisy. This effect is due to individual trees moving into and out of the path between the Sun and the sensors. This effect is most notable right at solar noon (about 31°), which is due to the larger effects of shadows cast by trunks and stems since the perches holding the sensors at each level were set up toward south and extend into the crowns. The second effect seen is that as solar zenith angle increases from solar noon, there is a general decline in transmittance as pathlength increases. The patches of alternately high and low transmittance correspond to local gaps and shadows specific to this location. Third, at very high solar zenith angles, transmittance increases. This effect is due to the high proportion of the illumination being diffuse skylight. Since the position of individual trees around sensors has less effect on the field measurements of diffuse skylight, this proportion of the graph shows less variability.

Both the original and the modified GORT model estimates exhibit the pattern of general decrease in transmission as solar zenith angle increases, until very high solar zenith angles where there is an increase. Note that the predicted minimum in transmittance occurs at slightly larger solar zenith angles than the measurements indicate. One possible reason for this shift could be errors in the estimated proportions of beam and diffuse skylight (see Figure 6). Also note that while the original GORT model captures the basic shape, it generally underestimates transmittance. The modification to incorporate the effect of whorls appears to produce better results.

The field measurements of PAR transmittance at the SOBS site (Figure 13) differ from the ones in the SOJP site (Figure 12). The PAR transmittance shows a sharp V shape around

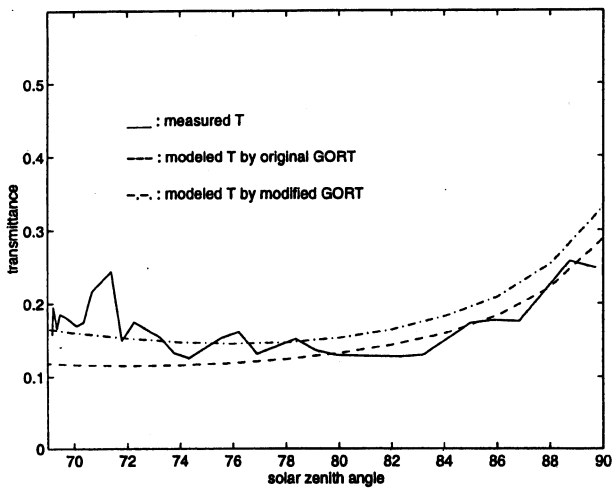

Figure 14. Comparison of modeled and measured total solar radiation transmission in the SOJP stand on days 38, 39, and 40 of 1994.

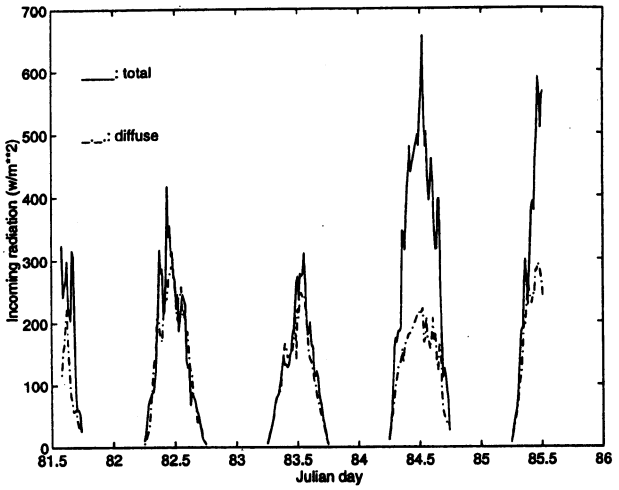

Figure 15. Incoming radiation in the NOBS stand on days 81, 82, 83, 84, 85 in 1995.

42°–45°, which is probably due to the effect of shadows from large groups of trees. This pattern results from the conditions at one location and thus is not very useful for evaluation of GORT estimates. However, when $\theta_i > 55°$, there is reasonable agreement between the field measurements and the prediction by GORT.

5.3. Total Solar Radiation Transmittance As a Function of Solar Zenith Angles

The PAR transmittance does not include the contribution of the multiple scattering within the canopy layer and the multiple bouncing between the canopy layer and the forest background. The pyranometer measurements at the forest floor in the snow-covered SOJP and NOBS sites made during BOREAS winter field campaigns enable evaluation of the prediction of total solar transmission by the GORT model. Figure 14 shows the comparison between the modeled and the measured total solar radiation transmittance as a function of solar zenith angles on clear days in the SOJP site. Estimates of transmittance from both the original and the modified GORT model match reasonably well with the field measurements.

The measurements in NOBS site were collected every 15 min on cloudy days. Figure 15 shows the contributions of the incident direct beam and diffuse skylight. Figure 16 shows the comparison of total solar radiation transmittance between the measurements and the estimates from the original and the modified GORT model. Good agreement between the field measurements and the estimates by the modified GORT model and a little underestimation by the original GORT model are indicated.

6. Discussion and Conclusion

Overall, this study shows that the combination of both GO and RT approaches to model the effect of conifer forest tree structure on the radiation transmission has advantages compared with either pure RT or pure GO approaches. The GO approach captures effects due to canopy gaps and self-shadowing. The RT approach accounts for the influence of the optical properties (leaf transmittance, reflectance, and absorption) of the foliage on multiple scattering. Moreover, the combination of these two approaches allows incorporation more easily of the complicated structure of conifer trees (e.g., accounting for the effect of the horizontal whorl structure).

The modeled radiation transmittance by GORT shows several effects of the conifer structure on the radiation transmission. First, a lower rate of radiation interception at the top of the canopy and a maximum in the upper or middle part of the canopy. This leads to a sigmoid shape for the vertical distribution PAR transmittance, which matches well with the field measurements. Beer's law fails to predict this shape. These transmission patterns indicate that more light will pass through the canopy and reach the lower part of the canopy. This is important for providing inputs for snowmelting models [see *Hardy et al.*, this issue] and with respect to the radiation available for photosynthesis in the lower branches. The cause of this transmission pattern is primarily the effect of the clumping of canopy elements, which can be modeled as the between-crown gap probability, which is directly linked with the tree geometry. This emphasizes a need for a detailed description of tree crown geometry and stem count density. Second, the effect of the horizontal whorl structure allows more light at larger solar zenith angles to pass through the canopy. Through incorporating this effect into the calculation of gap probabilities, comparison of the field measurements in the SOJP and NOBS sites for both total solar radiation and PAR transmittance with model estimates indicate that the modified GORT model is an improvement over the original GORT. Third, the effect of the clumping structure of conifer trees on the multiple scattering, as predicted by the GORT model, shows the maximum value in the upper or middle part of the canopy depending on the inclination angle of incident radiation. More multiple scattering occurs at larger solar zenith angles. Prediction of total solar radiation transmittance after considering the effect of multiple scattering agrees well with the field measurements in the snow-covered SOJP and NOBS test sites.

The test results in the SOBS site also showed some deviation of model estimates from the field measurements. At least part of the reason is due to the lognormal distribution of tree size in the SOBS site which deviates from assumptions in the GORT model. Incorporation of lognormal distributions of tree size into the GORT model is left for future work. There are

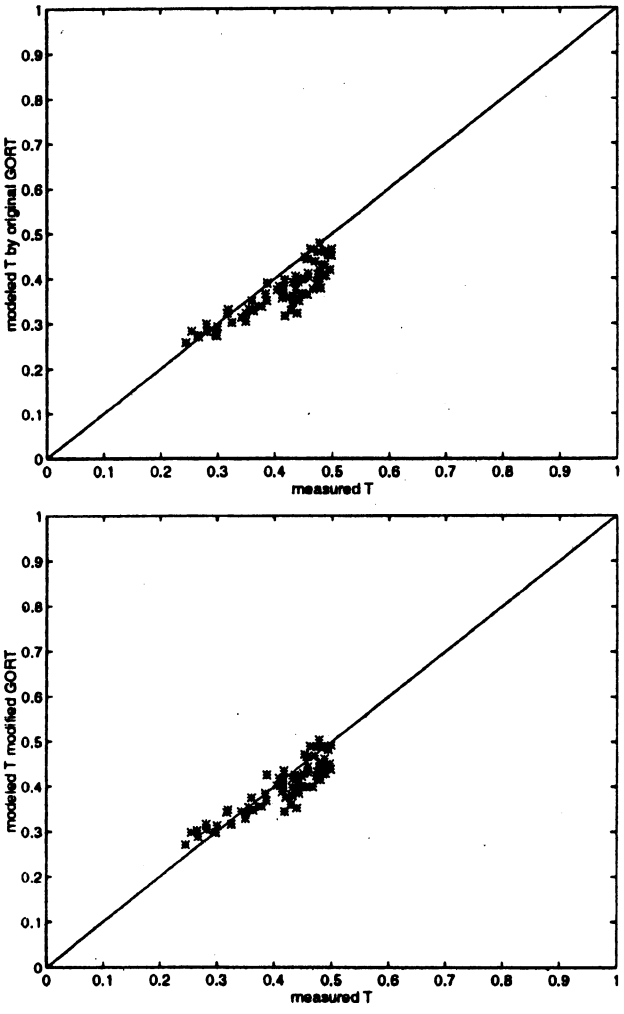

Figure 16. Measured (every 15 min) and predicted total solar radiation transmission by the original and modified GORT models in the NOBS stand on days 81, 82, 83, 84, 85 in 1995.

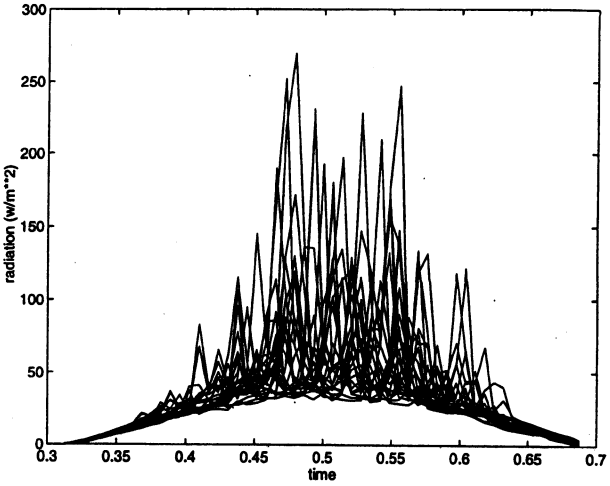

Figure 17. Three days of measurements from nine pyranometers at the SOJP stand, all normalized to local time, i.e., 0.5 at solar noon.

also a couple of other possible reasons for the disagreement between estimated transmittance and field measurements in the SOBS site. One is the effect of stems and branches and dead trees on the extinction coefficient. In this study, the extinction coefficient of the foliage is constant. A study in a Sitka spruce stand by *Norman and Jarvis* [1975] showed a sharp increase in extinction coefficients in the lowest region of the canopy, which is due to the proportionately larger effect of stems and branches. Another factor may be the effect of the shape of the tree crown. Some crowns may be cone shaped or even for an ellipsoid shape; the b/R ratio may be different for different size trees. More investigation of these factors is needed in the future.

One aspect of radiation measurements that is often overlooked in forests is the requirement for representative spatial sampling. The daily radiation from each pyranometer in the SOJP shown in Figure 17 clearly demonstrates the heterogeneity of radiation environments at the forest floor. It shows that measurements from a single location are insufficient to collect a representative sample. In an attempt to collect a representative sample, several pyranometers were located randomly at the SOJP and NOBS sites during the winter campaign, and the averaged values were used for validating GORT. Averaging the measurements from multiple locations minimizes the bias in measurements from a single location. For the PAR measurements in the SOJP and SOBS sites, although the measurements were collected at one location for each test site, measurements were collected throughout the summer (June to September). This allows for averaging of data with the same solar zenith angles, which will include a variety of solar azimuth angles over the course of the season. This substitution of temporal sampling for spatial sampling helps but does not completely remove the effects related to the positions of trees in the immediate vicinity of the sensors.

In general, models vary in complexity, as do expectations for precision in the estimates they produce. Clearly there are more complex models for the radiation environment in conifer forests, as mentioned in the background section. However, these more complex models (such as *Norman and Jarvis* [1975]) require considerably more input data on the structure of the canopy. The strength of the GORT model is that it can be parameterized at the stand scale by simply the stem count density, a few single tree geometry parameters, and characteristics of the irradiance. As such, it is possible to begin to distribute the model spatially by providing the necessary parameters for each stand. Hopefully, many of these parameters will be supplied from remote sensing. Ultimately, this approach allows landscape-scale analysis based on reasonably precise estimation of radiation properties at stand scales. The benefits of this approach in the context of snowmelt modeling is illustrated by the parametric study in another paper in this issue [*Davis et al.*, this issue].

An issue confronting future use of GORT concerns possible simplification to the model that would reduce computational requirements. This issue will become increasingly important in spatially distributed applications of GORT. For example, the multiple scattering within the canopy layer and multiple bouncing between the ground and the canopy layer in GORT were calculated on the basis of numerous numerical integrations. A newly derived, more simple formula for them can be test based on the numerical solution of GORT [*Li et al.*, 1996; W. Ni et al. (Decoupling path-scattering of light in a homogeneous layer

and multiple bouncing at its non-Lambertian bottom, submitted to *Journal of Geophysical Research*) 1996]. Also in GORT the within-crown gap probability is calculated by the summation of an exponential function of the pathlength distribution. However, the calculation of the within-crown gap probability can be simplified by an exponential function of the mean value of the pathlengths, resulting in considerable savings in computation. These issues of simplification of the model and the effect they have on the precision of the model will be addressed in future work.

Notation

a_0 branch orientation coefficient in $G_b(\theta_i)$.
b vertical crown radius (m).
$C(i, v)$ signature of sunlit crown surface.
L_e effective leaf area index ($m^2\ m^{-2}$).
F_a foliage volume density of a single crown (m^{-1}).
$G(i, v)$ signature of sunlit ground surface.
$G_b(\theta_i)$ branch orientation factor.
h, z certain height within the canopies (m).
h_c crown center height.
h_1 lower bound of the crown centers (m).
h_2 upper bound of the crown centers (m).
$k(\theta_i)$ leaf orientation factor.
$K_g(i, v)$ proportion of sunlit crown surface.
$K_c(i, v)$ proportion of sunlit ground surface.
$P(n = 0|h, \theta_i)$ between-crown gap probability for a beam at θ_i reaching height h.
$P(n > 0|h, \theta_i)$ within-crown gap probability for a beam at θ_i reaching height h.
$P(s|h, \theta_i)$ within-crown path length distribution for a beam at θ_i reaching height h.
$P(s|n, z, h, \theta_i)$ within-crown path length distribution for a beam at θ_i entering crowns at height z passing through n crowns, traveling to height h.
$P(n|z, h, \theta_i)$ distribution of numbers of crowns intercepted for a beam at θ_i entering crowns at height z, traveling to height h.
$P(s = 0|z, \theta_i)$ vertical distribution of sunlit crown surface for given angle θ_i.
R horizontal crown radius (m).
$R_e(i, v)$ bidirectional reflectance.
s within-crown path length.
s' beam path length.
$S(h, \theta_i)$ averaged path length within a single crown for a beam at θ_i traveling to height h.
V_{crown} single crown volume (m^3).
λ crown count density (m^{-2}).
λ_v crown count volume density (m^{-3}).
λ'_v crown count volume density in transformed dimension (m^{-3}).
ρ_I beam proportion.
$\tau(\theta)$ projected foliage area volume density at direction θ (m^{-1}).
θ_i solar zenith angle.
θ'_i solar zenith angle in the transformed dimension.
θ_v viewing zenith angle.
θ'_v viewing zenith angle in the transformed dimension.
γ_E the ratio of needle area in shoot-to-shoot area.

Appendix: Retrieving $G_b(\theta_i)$

The approach used here for retrieving $G_b(\theta_i)$ is empirical. On the basis of the fact that the leaf projection factor $k(\theta_i)$ at direction θ_i is equal to cos (θ_i) in a canopy with horizontal leaf orientation, the horizontal whorl branch structure parameter $G_b(\theta_i)$ at direction θ_i was assumed as

$$G_b(\theta_i) = a_0 \cos^2(\theta_i) + (1.0 - a_0) \quad \text{(A1)}$$

where the coefficient a_0 is to be adjusted. The above formula satisfies $G_b = 1.0$ at $\theta_i = 0°$ and G_b is a constant at $\theta_i = 90°$, which allows the grouping of shoots into branches. The value of a_0 was retrieved from PARABOLA data [*Deering*, 1995] in the SOJP site (notice that all the measurements are for solar zenith angle $\geq 35°$) by inverting a simplified geometric-optical mutual shadowing (GOMS) forest canopy reflectance model [*Li and Strahler*, 1992].

GOMS is a bidirectional reflectance model for discontinuous canopies derived from the GO approach. In the simplified version of GOMS model, it was assumed that the canopy reflectance for the nadir-viewed or hot spot cases is mainly the result of the reflectance (signature) of the sunlit canopy and sunlit ground surface, which can be expressed as

$$K_g(i, v)G(i, v) + K_c(i, v)C(i, v) = R_e(i, v) \quad \text{(A2)}$$

where $R_e(i, v)$ are the PARABOLA reflectance measurements, $G(i, v)$ and $C(i, v)$ are signatures of the sunlit and viewed ground and crown surface. The inverted signature values from *Li and Strahler* [1996] were used in this study. $K_g(i, v)$ and $K_c(i, v)$ are the areal proportions of the sunlit and viewed background and crown surface at illumination direction i and viewing direction v.

At large solar zenith angles the overlapping between illumination and viewing shadows of individual crowns as projected onto the background can be ignored. By considering the effect of the horizontal whorl branch structure on the sunlit and viewed ground surface area at the nadir-viewed case, $K_g(i, v)$ can be written as

$$K_g(i, v) = e^{-\lambda\pi R^2[G_b(\theta_i)\sec\theta'_i + \sec\theta'_v]} \quad \text{(A3)}$$

Also for the nadir-viewed case, the ratio of $F = K_c/1 - K_g$ is constant [*Li and Strahler*, 1992], where F can be expressed as

$$F = \frac{\frac{1}{2}(1 + \cos(\theta'_i))}{1.0 + \dfrac{G(\theta_i)}{\cos(\theta'_i)}}. \quad \text{(A4)}$$

For the hot spot case, the formulas for K_g and K_c reduce to

$$K_g(i, v) = e^{-\lambda\pi R^2 G_b(\theta_i)\sec\theta'_i} \quad \text{(A5)}$$

$$K_c(i, v) = 1 - K_g(i, v) \quad \text{(A6)}$$

where θ'_i and θ'_v are the transformed solar zenith angle θ_i and view zenith angle θ_v, with $\theta'_i = \tan^{-1}(b/R \tan\theta_i)$ and $\theta'_v = \tan^{-1}(b/R \tan\theta_v)$.

The unknown factors in our case are b/R, λR^2, and the coefficient a_0. Even with the field measurements of R, b, and

λ in the SOJP site, the bidirectional measurements may not be in exactly the same spot. However, within reasonable ranges of R, b, λ, and a_0 the inversion was implemented by finding the best set of values for $(b/R, \lambda R^2)$, and a_0 by the least mean squares (LMS) law. The inverted results are $a_0 = 0.7$, $\lambda R^2 = 0.18$, and $b/R = 3.1$, leading to $G_b(\theta_i) = 0.7 \cos^2(\theta_i) + 0.3$. In fact, a similar result was obtained through inversion of the full GOMS model using PARABOLA data [*Li and Strahler*, 1996].

Acknowledgments. This work was supported in part by U.S. Army Corps of Engineering under contract DACA89-93-k-00012, by NASA under contract NAS5-31369, and by China's NSF under grant 49331020. We also thank Meteo France and Programme National de Teledetection Spatiale (PNTS) for financial support. The authors are indebted to Janet Hardy, Susan Burak, Drew Pilant, and Bart Njissen for the field measurements and John Collins for the help with programming.

References

Bonan, G. B., F. S. Chapin III, and S. L. Thompson, Boreal forest and tundra ecosystem as components of the climate system, *Clim. Change*, *29*, 145–167, 1995.

Campbell, G. S., and Norman, J. M., The description and measurement of plant canopy structure, in *Plant Canopies: Their growth, form and function*, edited by R. Russell, B. Marshall, and P. G. Jarvis, Cambridge Univ. Press, New York, 1989.

Chen, J. M., Optically-based methods for measuring seasonable variation of leaf area index in boreal conifer stands, *Agric. For. Meteorol.*, *80*, 135–163, 1996.

Chen, J. M., T. A. Black, and R. S. Adams, Evaluation of hemispherical photography for determining plant area index and geometry of a forest stand, *Agric. For. Meteorol.*, *56*, 129–143, 1991.

Davis, R. E., C. J. McKenzie, J. P. Hardy, R. Jordan, W. Ni, X. Li, and C. Woodcock, Variation of snow cover ablation in the boreal forest: A sensitivity study on the effects of conifer canopy, *J. Geophys. Res.*, this issue.

Deering, D. W., Temporal attributes of the bidirectional reflectance for three boreal forest canopies, *Int. Geosci. Remote Sens. Symp.*, *2*, 1239–1241, 1995.

Dozier, J., Remote sensing of snow in visible and near-infrared wavelengths, *Theory and Application of Optical Remote Sensing*, edited by G. Asrar, John Wiley, New York, 1989.

Hammond, R., and P. S. McCullagh, *Quantitative Techniques in Geography: An Introduction*, Clarendon, Oxford, England, 1974.

Hardy, J. P., R. E. Davis, R. Jordan, X. Li, C. E. Woodcock, W. Ni, and J. C. MacKenzie, Snow ablation modeling at the stand scale in a boreal jack pine forest, *J. Geophys. Res.*, this issue.

Iqbal, M., *An Introduction to Solar Radiation*, Academic, San Diego, Calif., 1983.

Kimes, D. S., J. M. Norman, and C. L. Walthall, Modeling the radiative transfers of sparse vegetation canopies, *IEEE Trans. Geosci. Remote Sens.*, *23*, 695–704, 1985.

Kimes, D. S., W. W. Newcomb, R. F. Nelson, and J. B. Schutt, Directional reflectance distributions of a hardwood and pine forest canopy, *IEEE Trans. Geosci. Remote Sens.*, *24*, 281–293, 1986.

Li, X., and A. H. Strahler, Geometric-optical modeling of a conifer forest canopy, *IEEE Trans. Geosci. Remote Sens.*, *23*, 705–721, 1985.

Li, X., and A. H. Strahler, Geometric-optical bidirectional reflectance modeling of mutual shadowing effects of crowns in a forest canopy, *IEEE Trans. Geosci. Remote Sens.*, *30*, 276–292, 1992.

Li, X., and A. H. Strahler, A knowledge-based inversion of physical BRDF models and three case studies, *Int. Geosci. Remote Sens. Symp.*, 2173–2175, 1996.

Li, X., A. H. Strahler, and C. E. Woodcock, A hybrid geometric optical-radiative transfer approach for modeling albedo and directional reflectance of discontinuous canopies, *IEEE Trans. Geosci. Remote Sens.*, *33*, 466–480, 1995.

Li, X., W. Ni, C. Woodcock, and A. Strahler, A simplified hybrid model for radiation under discontinuous canopies, *Int. Geosci. Remote Sens. Symp.*, 293–295, 1996.

Middleton, E. M., and E. A. Walter-Shea, Optical properties of canopy elements in the boreal forest, *Int. Geosci. Remote Sens. Symp.*, 789–793, 1995.

Monsi, M., and T. Saeki, Über den Lichtfaktor in den Pflanzengesellschaften und seine Bedeutung für die Stoffproduction, *Jpn. J. Bot.*, *14*, 22–52, 1953.

Ni, W., A coupled transilience model for turbulent air flow in plant canopy and planetary boundary layer, *Agric. For. Meteorol.*, *86*, 77–105, 1997.

Nilson, T., A theoretical analysis of the frequency of gaps in plant stands, *Agric. Meteorol.*, *8*, 25–38, 1971.

Norman, J. M., and P. G. Jarvis, Photosynthesis in Sitka Spruce, III, Measurements of canopy structure and interception of radiation, *J. Appl. Ecol.*, *11*, 375–398, 1974.

Norman, J. M., and P. G. Jarvis, Photosynthesis in Sitka Spruce, V, Radiation penetration theory and a test case, *J. Appl. Ecol.*, *12*, 839–878, 1975.

Oker-Blom, S. Kellomaki, and H. Smolander, Photosynthesis of a Scots pine shoot: The effect of shoot inclination on the photosynthetic response subjected to direct radiation, *Agric. For. Meteorol.*, *29*, 191–206, 1983.

Oker-Blom, J. Lappi, and H. Smolander, Radiation regime and photosynthesis of coniferous stands, in *Photon-Vegetation Interactions—Application in Optical Remote Sensing and Plant Ecology*, edited by R. B. Myneni and J. Ross, Springer-Verlag, New York, 1991.

Ross, J. K., The Radiative Regime and Architecture of Plant Stands, 391 pp., Dr. W. Junk, Norwell, Mass., 1981.

Ross, J. K., and A. Marshak, Monte Carlo methods, in *Photon-Vegetation Interactions—Application in Optical Remote Sensing and Plant Ecology*, edited by R. B. Myneni and J. Ross, Springer-Verlag, New York, 1991.

Roujean, J. L., A tractable physical model of shortwave radiation interception by vegetative canopies, *J. Geophys. Res.*, *101*, 9523–9532, 1996.

Sampson, D. A., and F. W. Smith, Influence of canopy architecture on light penetration in lodgepole pine (*Pinus contorta var. latifolia*) forests, *Agric. For. Meteorol.*, *64*, 63–79, 1993.

Sellers, P., Canopy reflectance, photosynthesis and transpiration, *Int. J. Remote Sens.*, *6*, 1335–1372, 1985.

Sellers, P., Canopy reflectance, photosynthesis and transpiration, II, The role of biophysics in the linearity of their interdependence, *Remote Sens. Environ.*, *21*, 143–183, 1987.

Sellers, P., et al., The Boreal Ecosystem-Atmosphere Study (BOREAS): An overview and early results from the 1994 field year, *Bull. Am. Meteorol. Soc.*, *76*, 1549–1577, 1995.

Soffer, R. J., J. R. Miller, W. Wanner, and A. Strahler, Winter boreal forest canopy BRF results: Comparison between airborne data, laboratory simulations and geometrical-optical model data, *Int. Geosci. Remote Sens. Symp.*, *1*, 800–801, 1995.

Strahler, A. H., and D. L. B. Jupp, Modeling bidirectional reflectance of forests and woodlands using Boolean models and geometric optics, *IEEE Remote Sens. Environ.*, *30*, 276–292, 1990.

Urban, D. L., R. U. O'Neill, and H. H. Shugart Jr., Landscape ecology, *Bioscience*, *37*, 119–127, 1987.

R. E. Davis, Cold Regions Research Engineering Laboratory, U.S. Army Corps of Engineers, 72 Lyme Road, Hanover, NH 03755.

X. Li, W. Ni, and C. E. Woodcock, Department of Geography and Center for Remote Sensing, Boston University, 725 Commonwealth Avenue, Boston, MA 02215.

J.-L. Roujean, GAME/CNRM (Meteo France, CNRS), 42 Avenue Gustave Coriolis, 31057 Toulouse Cedex, France.

(Received July 1, 1996; revised December 2, 1996;
accepted December 21, 1996.)